ACS APPLIED MATERIALS & INTERFACES

Research Article

www.acsami.org

Thermal Atomic Layer Etching of SiO_2 by a "Conversion-Etch" Mechanism Using Sequential Reactions of Trimethylaluminum and Hydrogen Fluoride

Jaime W. DuMont,[†] Amy E. Marquardt,[†] Austin M. Cano,[†] and Steven M. George*[,†,‡]

[†]Department of Chemistry and Biochemistry, and [‡]Department of Mechanical Engineering, University of Colorado at Boulder, Boulder, Colorado 80309, United States

ABSTRACT: The thermal atomic layer etching (ALE) of SiO_2 was performed using sequential reactions of trimethylaluminum (TMA) and hydrogen fluoride (HF) at 300 °C. Ex situ X-ray reflectivity (XRR) measurements revealed that the etch rate during SiO_2 ALE was dependent on reactant pressure. SiO_2 etch rates of 0.027, 0.15, 0.20, and 0.31 Å/cycle were observed at static reactant pressures of 0.1, 0.5, 1.0, and 4.0 Torr, respectively. Ex situ spectroscopic ellipsometry (SE) measurements were in agreement with these etch rates versus reactant pressure. In situ Fourier transform infrared (FTIR) spectroscopy investigations also observed SiO_2 etching that was dependent on the static reactant pressures. The FTIR studies showed that the TMA and HF reactions displayed self-limiting behavior at the various reactant pressures. In addition, the FTIR spectra revealed that an Al_2O_3/aluminosilicate intermediate was present after the TMA exposures. The Al_2O_3/aluminosilicate intermediate is consistent with a "conversion-etch" mechanism where SiO_2 is converted by TMA to Al_2O_3, aluminosilicates, and reduced silicon species following a family of reactions represented by $3SiO_2 + 4Al(CH_3)_3 \rightarrow 2Al_2O_3 + 3Si(CH_3)_4$. Ex situ X-ray photoelectron spectroscopy (XPS) studies confirmed the reduction of silicon species after TMA exposures. Following the conversion reactions, HF can fluorinate the Al_2O_3 and aluminosilicates to species such as AlF_3 and SiO_xF_y. Subsequently, TMA can remove the AlF_3 and SiO_xF_y species by ligand-exchange transmetalation reactions and then convert additional SiO_2 to Al_2O_3. The pressure-dependent conversion reaction of SiO_2 to Al_2O_3 and aluminosilicates by TMA is critical for thermal SiO_2 ALE. The "conversion-etch" mechanism may also provide pathways for additional materials to be etched using thermal ALE.

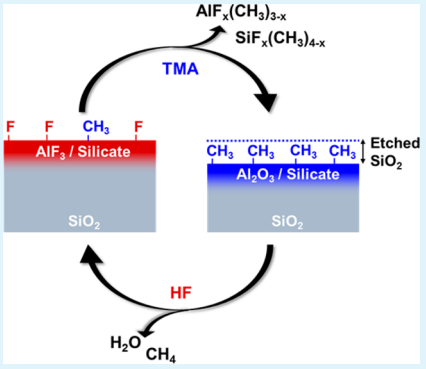

KEYWORDS: *atomic layer etching, SiO_2, trimethylaluminum, hydrogen fluoride, Al_2O_3, aluminosilicate*

I. INTRODUCTION

Silicon dioxide (SiO_2) is the most abundant mineral in the Earth's crust. SiO_2 is also an important semiconductor material. SiO_2 has many uses, such as for a gate oxide, interlayer dielectric or spacer, in semiconductor devices. SiO_2 etching is needed for multiple steps during semiconductor manufacturing.[1] The progressive miniaturization of semiconductor devices to sub-10 nm dimensions has imposed more demanding requirements on etching. As device structures become increasingly smaller and more complex, high precision etching is necessary at the sub-1 nm level using atomic layer etching (ALE) methods.[2]

There are many approaches for SiO_2 etching using HF/H_2O solutions, HF/H_2O vapor mixtures, and halogen plasmas. Etching SiO_2 in aqueous HF solutions is one of the oldest and useful SiO_2 etching methods.[3] The overall chemical reaction during SiO_2 etching in HF solutions is $SiO_2 + 6HF \rightarrow H_2SiF_6 + 2H_2O$.[4,5] The mechanism of SiO_2 etching in HF solutions involves the progressive fluorine replacement of hydroxyl groups on Si−OH silanol surface species using HF or HF_2^- to form Si−F surface species.[4−6] H_2O or HF can also break the Si−O−Si siloxane linkage in SiO_2 to produce additional Si−OH silanol and Si−F surface species.

SiO_2 can also be etched by HF/H_2O in the gas phase. The gas phase approach is an extension of the solution phase approach and occurs when H_2O and HF are present at pressures sufficient to form a condensed HF/H_2O layer on the SiO_2 surface.[7,8] H_2O is essential for HF etching of SiO_2.[9] Vapor phase SiO_2 etch rates are in agreement with the etch rates expected from the composition of the condensed HF/H_2O layer present at the given HF and H_2O partial pressures.[7] The chemistry of vapor phase SiO_2 etching is the same as observed in aqueous HF solutions. In addition, H_2SiF_6 is removed by the reaction $H_2SiF_6 \rightarrow SiF_4 + 2HF$.[7]

Fluorocarbon-based plasma etching can also be employed for SiO_2 etching.[10−12] F atoms in the plasma have been identified as the active etching reactant. SiF_4 has been detected as the main Si-containing reaction product. Fluorocarbon plasmas are also used in newly developed plasma ALE methods based on an Ar plasma producing low energy Ar^+ ions together with a periodic fluorocarbon-based plasma exposure.[13,14] The fluorocarbon-based plasma deposits a fluorocarbon layer on the

Received: January 24, 2017
Accepted: February 27, 2017
Published: February 27, 2017

DOI: 10.1021/acsami.7b01259
ACS Appl. Mater. Interfaces 2017, 9, 10296−10307

SiO_2 surface. The Ar^+ ion bombardment then desorbs the fluorocarbon layer and also removes a controlled amount of the SiO_2 layer.

Thermal ALE processes have been introduced recently for Al_2O_3, HfO_2, ZrO_2, AlF_3, and AlN ALE based on sequential fluorination and ligand-exchange reactions.[15−22] In these thermal reactions, the metal oxide is first fluorinated to produce the metal fluoride.[17,19,22] The metal fluoride is then removed by a metal precursor in a ligand-exchange transmetalation reaction.[17,19,22] In this ligand-exchange reaction, the metal precursor accepts fluorine from the metal fluoride and donates one of its ligands to the metal fluoride. The resulting reaction product formed from the metal fluoride can then desorb from the surface if this metal species is stable and volatile.[20,22]

In this paper, a new gas-phase thermal SiO_2 ALE process is reported based on sequential exposures of $Al(CH_3)_3$ (trimethylaluminum (TMA)) and HF. SiO_2 film thicknesses were measured versus number of ALE cycles using ex situ spectroscopic ellipsometry to obtain the SiO_2 etching rates. These studies determined the linearity of the SiO_2 etching and the dependence of the SiO_2 etching on the TMA and HF reactant pressures. Ex situ X-ray photoelectron spectroscopy (XPS) measurements were also employed to determine the silicon oxidation state after the TMA and HF reactions. In addition, in situ Fourier transform infrared (FTIR) spectroscopy measurements were used to measure the loss of absorbance from Si−O stretching vibrations and to monitor the surfaces species present after each TMA and HF exposure at various pressures.

Recent studies of ZnO ALE using TMA and HF as the reactants have revealed a new "conversion-etch" reaction mechanism where a ZnO surface layer is converted to an Al_2O_3 surface layer and volatile $Zn(CH_3)_2$ reaction products during the TMA exposure.[23] In this investigation, the FTIR and XPS studies determined that there was a similar conversion of SiO_2 to Al_2O_3 by TMA. The observation of Al_2O_3, aluminosilicate species, and silicon in reduced oxidation states established that the "conversion-etch" mechanism also occurs for SiO_2 ALE. In addition, the reactant pressures were critical for SiO_2 ALE and larger etch rates occurred at higher reactant pressures. The generality of the "conversion-etch" mechanism could expand the number of materials that can be etched using thermal ALE methods.

II. EXPERIMENTAL SECTION

1. Static Reactor, Silicon Wafers, and Ex Situ Film Analysis. ALE reactions were performed in a hot wall ALD reactor.[24] A proportional-integral-derivative (PID) temperature controller (2604, Eurotherm) maintained the reaction temperature at 300 °C. A capacitance manometer (Baratron 121A, MKS) monitored the pressure in the reactor. The starting SiO_2 substrate was a thermal SiO_2 layer with a thickness of 40 nm on Si(100) wafers with a diameter of 100 mm (University Wafer). The silicon wafers were cut into samples with dimensions of 2.5 cm × 2.5 cm before the SiO_2 ALE.

The SiO_2 ALE reactions were accomplished using sequential static exposures of TMA (97%, Sigma-Aldrich) and HF derived from HF−pyridine (70 wt % HF, Sigma-Aldrich). HF−pyridine was transferred to a gold-plated stainless steel bubbler using a dry N_2-filled glovebag. The TMA and HF−pyridine precursors were held at room temperature. Each reactant exposure consisted of a static dose of 20 s followed by a purge of 120 s with 550 sccm of ultrahigh purity (UHP) N_2. The total N_2 gas flow of 550 sccm produced a base pressure of ∼2 Torr in the reactor during the purge steps. The N_2, precursor, and reaction byproducts were pumped by a mechanical pump (Pascal 2010SD, Alcatel Adixen).

The ex situ X-ray reflectivity (XRR) scans were measured by a high resolution X-ray diffractometer (Bede D1, Jordan Valley Semiconductors) using Cu Kα (λ = 1.540 Å) radiation. The filament voltage and current in the X-ray tube were 40 kV and 35 mA, respectively. A 5 arcsec step size and a 10 s acquisition time were used for recording all XRR scans with a range of 300−4500 arcsec. The analysis software (Bede REFS, Jordan Valley Semiconductors) determined film thickness, film density, and surface roughness by fitting the XRR scans.

Ellipsometry was performed using a spectroscopic ellipsometer (J. A. Woollam M-2000D). This ellipsometer has a spectral range of 240−1700 nm and utilizes an incidence angle of 75°. A Cauchy model was used to determine the film thickness. This modeling was performed using analysis software (CompleteEASE, J. A. Woollam). SiO_2 film thicknesses were measured at the same position on each silicon sample before and after etching.

Thermal SiO_2 layers with a thickness of 40 nm on Si(100) wafers (University Wafer) were used for XPS analysis to determine the surface species after TMA-only and TMA/HF exposures. These SiO_2 samples were exposed to 8 Torr of TMA for 5 min or 8 Torr of TMA for 5 min followed by 4 Torr of HF for 10 min. After the static reactant exposures, the samples were immediately transferred to a PHI 5600 X-ray photoelectron spectroscopy (XPS) spectrometer to analyze the films. A SiO_2 sample without TMA or HF exposures was also analyzed with XPS.

A monochromatic Al Kα X-ray source (1486.6 eV) was used to collect survey scans with a pass energy of 93.9 eV and step size of 0.400 eV. An XPS software package (Auger Scan, RBD Instruments) was used to collect the XPS spectra. Casa XPS software (Casa XPS, Casa Software) was used for peak analysis of the C 1s, O 1s, Si 2p, Al 2p, and F 1s XPS signals. All peaks were calibrated to the C 1s peak centered at 284.8 eV.

The oxidation state of Si was determined through fitting the Si 2p peak profile using Gaussian−Lorentzian line shapes after a Shirley background subtraction. XPS analysis of the SiO_2 control sample was used to determine the Si 2p binding energy position and full width at half-maximum (fwhm) of the 4+ oxidation state peak. The binding energy (104.3 eV) and fwhm (2.1 eV) of the 4+ oxidation state were imposed in the fittings of the TMA-only and TMA/HF exposed samples. The binding energy positions for the 3+, 2+, 1+, and 0 oxidation states were defined as −1, −2, −3, and −4 eV with respect to the 4+ peak.[25,26] The fwhm values of the 3+, 2+, 1+, and 0 oxidation states were set to 1.2 ± 0.1, 1.1 ± 0.1, 1.0 ± 0.1, and 1.0 ± 0.1 eV, respectively.[25−27]

2. In Situ Fourier Transform Infrared (FTIR) Spectroscopy Studies. The surface chemistry during sequential exposures of TMA (97%, Sigma-Aldrich) and HF derived from HF−pyridine (70 wt % HF, Sigma-Aldrich) on SiO_2 at 300 °C was studied using in situ FTIR spectroscopy. The in situ FTIR studies were performed in a reactor equipped with an FTIR spectrometer that has been described previously.[28] The FTIR experiments utilized high surface area Si nanoparticles (>98%, US Research Nanomaterials) with an average diameter of 20−30 nm. The large surface area provided by the nanopowder sample improved the signal-to-noise ratio for infrared absorption. The Si nanoparticles were mechanically pressed into a tungsten grid support to facilitate the transmission FTIR measurements.[29] The tungsten grid was 2 × 3 cm^2, 50 μm thick, with 100 grid lines per inch.

The tungsten grid could be resistively heated using a dc power supply (6268B, 20 V/20 A, Hewlett-Packard). The voltage output of the power supply was controlled by a PID temperature controller (Love Controls 16B, Dwyer Instruments). A type K thermocouple was attached to the bottom of the tungsten grid with epoxy (Ceramabond 571, Aremco) that attached and electrically isolated the thermocouple. To create a uniform SiO_2 surface, the Si nanoparticles were annealed at 650 °C for 1 h under ∼25 Torr of H_2O vapor.

Figure 1a shows the absolute FTIR spectra of the SiO_2 coating on the Si nanoparticles before and after the H_2O oxidation process.

DOI: 10.1021/acsami.7b01259
ACS Appl. Mater. Interfaces 2017, 9, 10296−10307

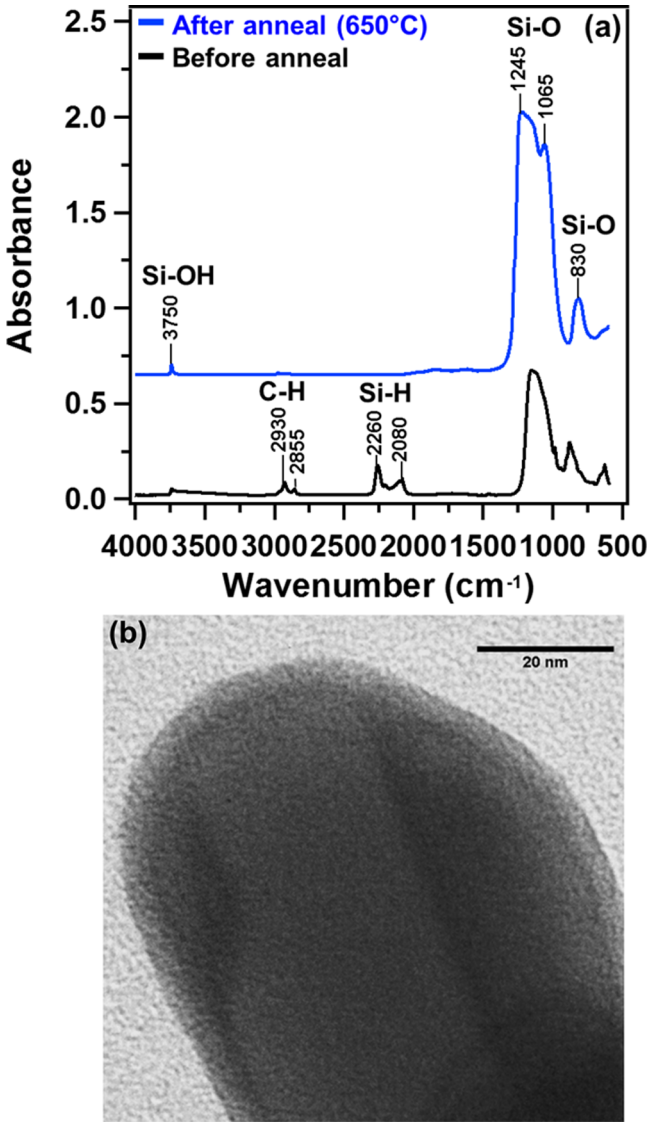

Figure 1. (a) Absolute FTIR spectra of silicon particles with a SiO_2 coating before and after oxidation with ~25 Torr H_2O at 650 °C for 1 h. (b) TEM image of a silicon nanoparticle with a ~3.5 nm thick SiO_2 coating after the H_2O thermal oxidation.

Distinctive absorption features for the unannealed sample are observed in four frequency regions: 835−1250 cm^{-1}, 2080−2260 cm^{-1}, 2855−2930 cm^{-1}, and 3250−3750 cm^{-1}. The strong and broad absorption bands between 835 and 1250 cm^{-1} are consistent with the TO/LO modes that arise from Si−O symmetric and asymmetric stretching vibrations.[30] The absorption bands observed between 2080 and 2260 cm^{-1} are attributed to SiH_x and SiO_xH_{3-x} species.[31−33] Absorption bands between 2855 and 2930 cm^{-1} are attributed to the C−H stretching vibrations of adventitious hydrocarbons. The broad absorption feature observed between 3250 and 3750 cm^{-1} is consistent with isolated and hydrogen bonded Si−OH species. These results are in agreement with a partially oxidized hydrogen-terminated silicon surface.

After thermal oxidation with H_2O, evidence of silicon oxidation is observed in each distinctive absorption band. Between 835 and 1250 cm^{-1}, large absorbance gains are observed that are consistent with the addition of bulk Si−O−Si stretching vibrations. These results are consistent with previous studies that have demonstrated the formation of a thermal oxide layer on silicon surfaces exposed to water vapor at elevated temperatures.[34,35] Furthermore, a distinct blue shift from 1045 to 1065 cm^{-1} and from 1160 to 1245 cm^{-1} is observed for the TO/LO modes after thermal oxidation. This behavior has been observed previously and is related to the stoichiometry of the SiO_x film. As more oxygen is incorporated into the film, a more electronegative environment leads to shorter Si−O bonds lengths and higher stretching frequencies.[30]

The disappearance of the vibrational features between 2080 and 2260 cm^{-1} is attributed to Si−H removal via H_2 evolution. H_2 desorption has been shown to occur on hydrogen-covered Si surfaces at 325−625 °C.[36,37] Thermal Si−H removal results in Si surface dangling bond sites that are susceptible to oxidation.[32,38,39] Absorption features between 2855 and 2930 cm^{-1} are also lost due to the volatilization of the carbon contaminants in the oxidizing environment. Lastly, there is an absorbance gain observed at 3750 cm^{-1} that is attributed to the formation of isolated Si−OH species. Previous studies have also observed the formation of isolated Si−OH species during oxidation of hydrogen-passivated silicon surfaces.[32]

This H_2O thermal oxidation procedure consistently removed any carbon-related vibrational modes and resulted in a SiO_2 coating on the Si nanoparticles with absorbances attributed only to the O−H hydroxyl stretching vibrations and bulk SiO_2 vibrational features. Transmission electron microscopy (TEM) analysis was utilized to confirm the presence of the SiO_2 coating on the Si nanoparticles. Figure 1b shows the TEM image of an annealed silicon nanoparticle with a SiO_2 coating with a thickness of ~3.5 nm. The SiO_2 coating is very uniform and conformal on the Si nanoparticle.

III. RESULTS AND DISCUSSION

1. 1. X-ray Reflectivity Measurements of SiO_2 Etching.

Figure 2 displays XRR measurements of the change in the SiO_2 film thickness versus ALE cycles at 300 °C for various static reactant pressures. The reaction sequence was defined by reactant exposures with a duration of 20 s and purges with a duration of 120 s. This reaction sequence is designated 20−120−20−120. The reactant pressures for the TMA and HF exposures were the same. The initial SiO_2 thermal oxide film on the silicon samples had a thickness between 390 and 397 Å.

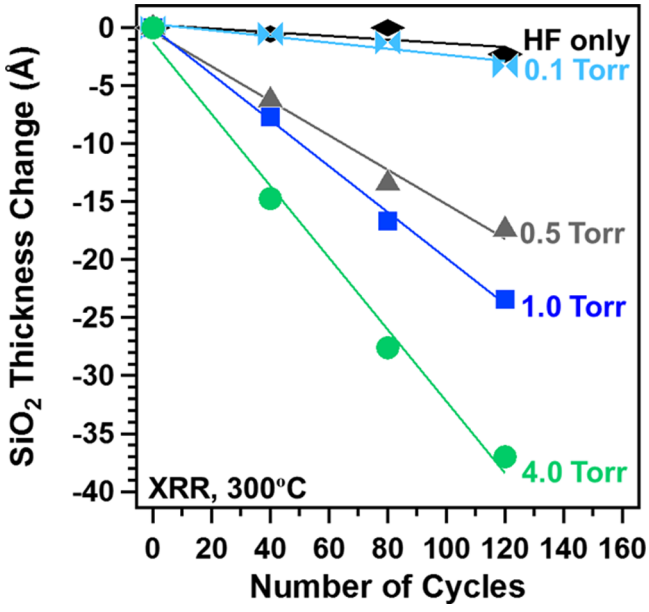

Figure 2. SiO_2 film thickness change versus number of SiO_2 ALE cycles determined by X-ray reflectivity measurements at TMA/HF pressures of 0.1, 0.5, 1.0, and 4.0 Torr. HF only experiments were also performed using an HF pressure of 1.0 Torr.

Figure 2 shows that the SiO_2 film thickness change versus number of ALE cycles is linear at each reactant pressure. The

DOI: 10.1021/acsami.7b01259
ACS Appl. Mater. Interfaces 2017, 9, 10296−10307

SiO_2 etch rates were 0.027, 0.15, 0.20, and 0.31 Å/cycle for static reactant pressures of 0.1, 0.5, 1.0, and 4.0 Torr, respectively. Previous results that utilized lower reactant pressures of ~0.08 Torr in a viscous flow mode showed no SiO_2 etching by TMA and HF at 300 °C.[18] The larger SiO_2 etch rates observed at higher precursor pressures suggest a pressure-dependent reaction mechanism for SiO_2 ALE.

Control experiments were also performed using only HF exposures of 1.0 Torr. The results in Figure 2 indicate that HF exposures by themselves resulted in negligible etching of the SiO_2 film at 300 °C. These results are consistent with earlier results that concluded that HF alone cannot etch SiO_2.[7,9] H_2O vapor needs to be present together with HF for SiO_2 etching.

2. Spectroscopic Ellipsometry Measurements of SiO_2 Etching. Figure 3 displays SE measurements of the change in the SiO_2 film thickness versus ALE cycles at 300 °C for various static reactant pressures. The reaction sequence was defined by reactant exposures with a duration of 20 s and purges with a duration of 120 s. The reactant pressures for the TMA and HF exposures were the same. The initial SiO_2 thermal oxide film on the silicon samples had a thickness between 390 and 397 Å.

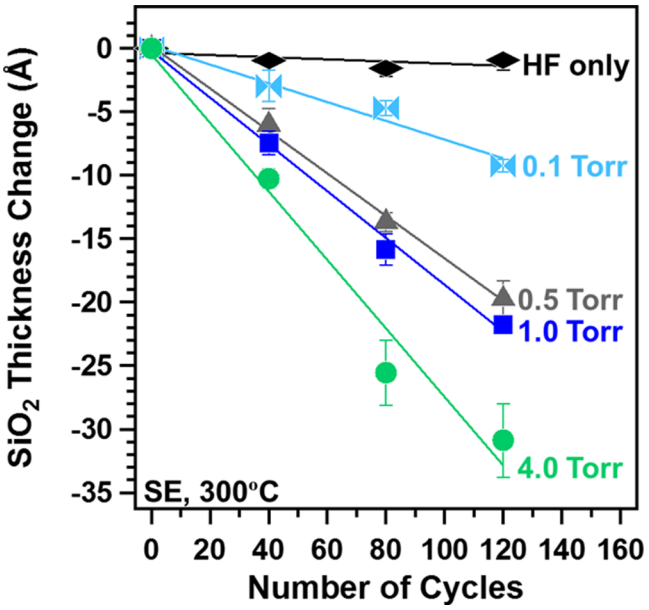

Figure 3. SiO_2 film thickness change versus number of SiO_2 ALE cycles determined by spectroscopic ellipsometry measurements at TMA/HF pressures of 0.1, 0.5, 1.0, and 4.0 Torr. HF only experiments were also performed using an HF pressure of 1.0 Torr.

Figure 3 shows that the SiO_2 film thickness change versus number of ALE cycles is linear at each reactant pressure. The etch rates were 0.07, 0.17, 0.18, and 0.27 Å/cycle for static reactant pressures of 0.1, 0.5, 1.0, and 4.0 Torr, respectively. The etch rates from the SE measurements are in good agreement with the etch rates from the XRR measurements. Control experiments were also performed using only HF exposures of 1.0 Torr. The results in Figure 3 demonstrate that only HF exposures lead to negligible SiO_2 etching.

3. FTIR Spectroscopy Measurements of SiO_2 Etching. Figure 4 displays the absolute FTIR spectra from 700 to 1500 cm^{-1} for Si particles covered with a SiO_2 coating during static TMA and HF exposures at 0.5, 1, and 4 Torr at 300 °C. Each reactant exposure consisted of a static dose at the specified pressure for 30 s followed by a 240 s purge. The most prominent vibrational features are attributed to the transverse optical (TO) and longitudinal optical (LO) modes arising from asymmetric Si−O stretching vibrations of SiO_4 tetrahedra at 1065 and 1230 cm^{-1}, respectively.[30] The less intense peak at 820 cm^{-1} is attributed to the corresponding TO and LO modes arising from symmetric Si−O stretching vibrations.[30] The absorbance features from the Si−O stretching vibrations decrease progressively versus the number of ALE cycles. An absorbance feature also appears at 1275 cm^{-1} after the first TMA exposure that is attributed to a deformation mode of Si−CH_3 surface species.[40] This result is consistent with previous studies that have observed the formation of Si−CH_3 species during reactions of TMA with SiO_2 surfaces.[41−43]

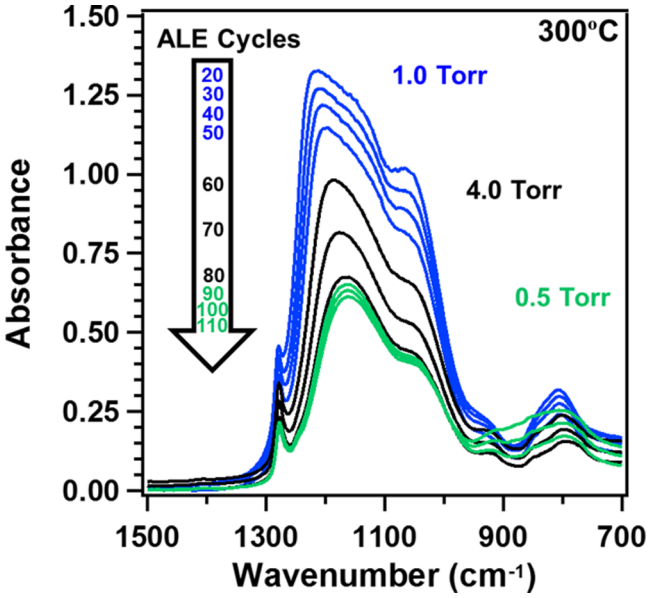

Figure 4. Absolute FTIR spectra showing the absorbance loss from Si−O stretching vibrations between 700 and 1500 cm^{-1} versus SiO_2 ALE cycles at TMA/HF pressures of 0.5, 1.0, and 4.0 Torr at 300 °C.

The FTIR spectra in Figure 4 were recorded after the TMA exposures. The first 50 cycles consisted of static reactant exposures at 1 Torr and showed a progressive loss of the absorbance for the Si−O stretching vibrations versus the number of ALE cycles. The nanoparticles were subsequently exposed to 30 cycles of static reactant exposures at 4 Torr and then 30 cycles of static reactant exposures at 0.5 Torr. The absorbance change per cycle of the Si−O stretching vibrations increased significantly at 4 Torr. This more rapid absorbance change indicates a larger SiO_2 etch rate at the higher reactant pressure. The absorbance change per cycle then decreased during the subsequent 0.5 Torr static exposures.

The absolute integrated absorbances of the asymmetric Si−O stretching vibrations between 900 and 1400 cm^{-1} versus ALE cycle number are plotted in Figure 5. At each pressure, the absorbance decreases linearly versus sequential TMA and HF exposures. ΔAbs/cycle values of −1.1, −1.9, and −3.6 are obtained for reactant pressures of 0.5, 1, and 4 Torr, respectively. These results are in agreement with the ex situ XRR and SE measurements that revealed larger SiO_2 etch rates at higher reactant pressures.

The etch rates and absorbance losses per cycle versus reactant pressure obtained by XRR, SE, and FTIR measurements are plotted in Figure 6. The relative etch rates determined by XRR and SE measurements at various reactant

DOI: 10.1021/acsami.7b01259
ACS Appl. Mater. Interfaces 2017, 9, 10296−10307

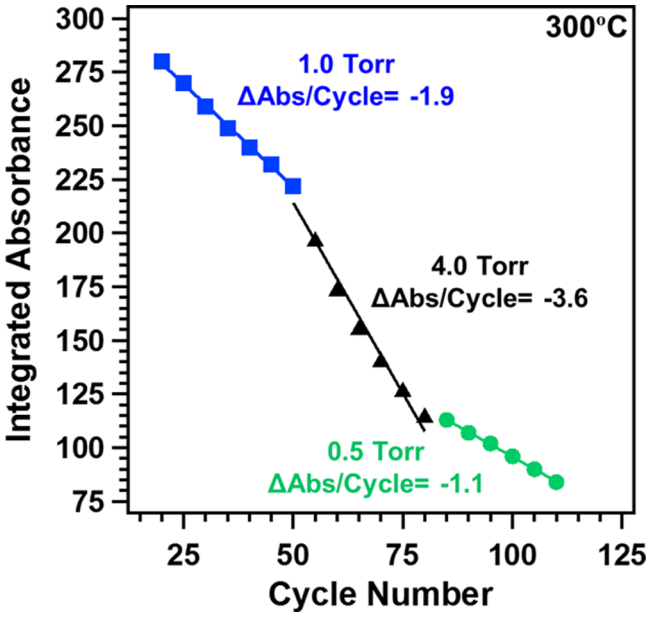

Figure 5. Absolute integrated absorbance of the Si−O stretching vibrations between 900 and 1400 cm^{-1} versus ALE cycle number at TMA/HF pressures of 0.5, 1.0, and 4.0 Torr. The integrated absorbance change per cycle was −1.1, −1.9, and −3.6 at pressures of 0.5, 1.0, and 4.0 Torr, respectively.

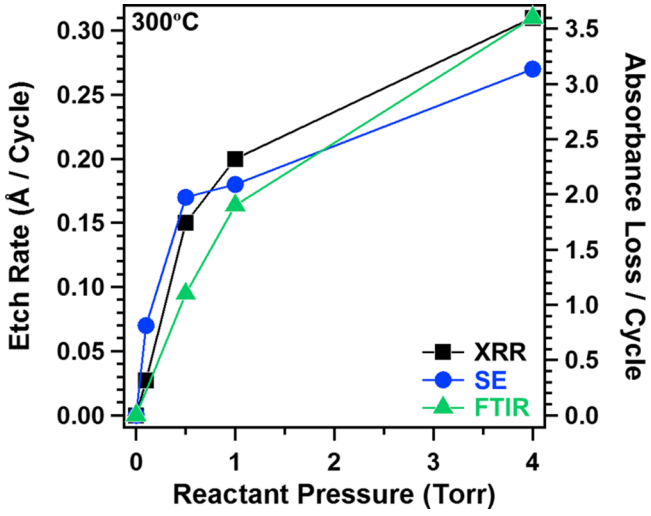

Figure 6. Etch rates from the XRR measurements in Figure 2 and the SE measurements in Figure 3 compared with the absorbance loss versus cycle from Figure 5 versus reactant pressure.

pressures are in good agreement with the absorbance loss per cycle determined using FTIR spectroscopy. All of the measurement techniques showed that the etch rate increases up to 1 Torr and then begins to level off at higher pressures. The leveling off of the etch rate at higher pressures suggests a diffusion-limited process similar to the oxidation of silicon substrates.[34] The surface layers formed during either the TMA or HF reactions act as diffusion barriers. These surface layers progressively limit the transport of reactants as the thickness of the surface layer increases.

4. FTIR Studies of Surface Chemistry and Thin Film Changes. The FTIR spectra can examine the surface chemistry and thin film changes during SiO_2 ALE. Figure 7 displays the FTIR difference spectra between 500 and 1700 cm^{-1} for the

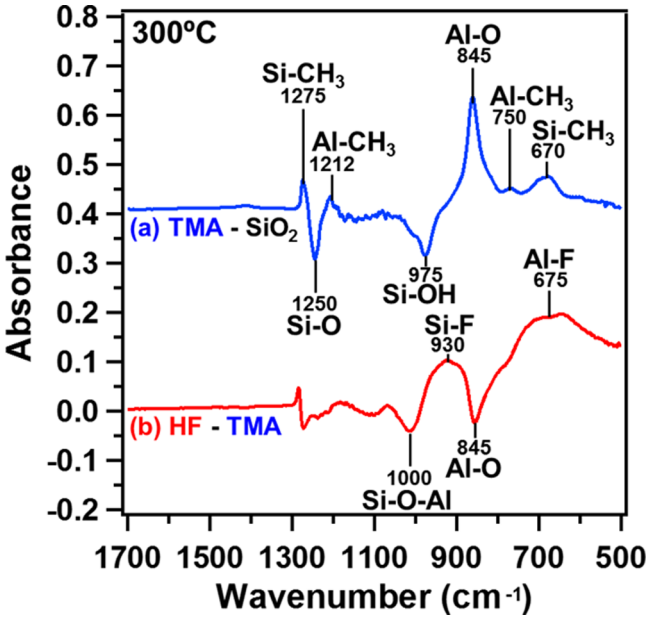

Figure 7. Difference infrared absorbance spectra from 500−1700 cm^{-1} during the first TMA and HF exposures on SiO_2 at 300 °C. (a) Spectrum after the first TMA exposure referenced to the spectrum for the initial SiO_2 layer on the silicon particles. (b) Spectrum after the first HF exposure referenced to the spectrum after the first TMA exposure.

first TMA and HF exposures on SiO_2 at 300 °C. Each reactant exposure consisted of a ∼1 Torr static dose for 30 s followed by a purge for 240 s. Figure 7a shows the difference spectrum defined by the spectrum recorded after the first TMA exposure referenced to the spectrum of the initial SiO_2 coating on the Si particles (TMA − SiO_2). Negative absorbance features at 975 and 1250 cm^{-1} are observed that are consistent with the loss of Si−OH and Si−O species, respectively.[30,44] These absorbance losses are accompanied by absorbance gains at 670, 750, 845, 1212, and 1275 cm^{-1}.

The absorbance gains at 670 and 1275 cm^{-1} in Figure 7a are attributed to the addition of $Si-CH_3$ species.[41,45] The absorbance gains at 750 and 1212 cm^{-1} are consistent with the addition of $Al-CH_3$ species. The absorbance gain at 845 cm^{-1} is assigned to the formation of Al−O species.[46−48] The resulting surface could contain $AlO_{3-x}(CH_3)_x$ species where x = 1 or 2 and $SiO_{4-y}(CH_3)_y$ species where y = 1, 2, or 3. These FITR measurements are in agreement with previous studies that have reported that TMA chemisorbs on silica surfaces primarily through reaction with hydroxyl groups and siloxane bridges.[41,43,49] TMA reactions with hydroxyl groups result in the formation of siloxy-methylaluminum surface species and methane. During dissociation of TMA on siloxane bridges, methyl groups are transferred from aluminum to silicon.

Figure 7b displays the infrared difference spectrum after the subsequent HF exposure. The Si−O−Al and Al−O vibrational features that were added during the previous TMA exposure are lost after the subsequent HF exposure. These absorbance losses are accompanied by absorbance gains at 675 and 930 cm^{-1} that are consistent with Al−F and Si−F species, respectively.[50,51] These results suggest that the Al−O species and Si−O−Al species formed during the TMA exposures are converted to Al−F and Si−F species during HF exposures, respectively. The reaction of HF with Al_2O_3 to produce AlF_3 has been observed in previous ALE studies.[17−19] This reaction occurs as

DOI: 10.1021/acsami.7b01259
ACS Appl. Mater. Interfaces 2017, 9, 10296−10307

$$Al_2O_3 + 6HF \rightarrow 2AlF_3 + 3H_2O \quad (1)$$

Thermochemical calculations indicate that this reaction is spontaneous at 300 °C with a Gibbs free energy value of $\Delta G = -41.1$ kcal.[52]

Figure 8 shows the FTIR difference spectra between 500 and 1700 cm^{-1} for two consecutive TMA and HF exposures

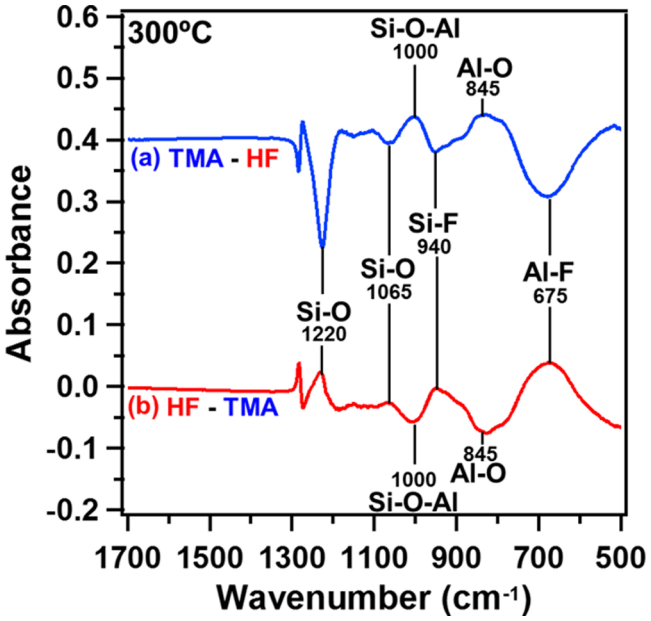

Figure 8. Difference infrared absorbance spectra from 500 to 1700 cm^{-1} during the sixth ALE cycle at 300 °C. (a) Spectrum after the sixth TMA exposure referenced to the spectrum after the fifth HF exposure. (b) Spectrum after the sixth HF exposure referenced to the spectrum after the sixth TMA exposure.

recorded during the sixth ALE cycle at 300 °C. These difference spectra are referenced using the spectra after the previous reactant exposure and are displaced for clarity in presentation. Each reactant exposure consisted of a ~1 Torr static dose for 30 s followed by a purge for 240 s. Figure 8a displays the difference spectrum after the TMA exposure referenced to the spectrum collected after the previous HF exposure (TMA − HF).

After TMA exposures, a broad absorbance loss is observed at 675 cm^{-1} that is consistent with the removal of Al−F stretching vibrations.[51] Etching of AlF_3 has been observed between 250 and 300 °C using TMA.[16,18] The etching of AlF_3 is consistent with the reaction

$$AlF_3 + 2Al(CH_3)_3 \rightarrow 3AlF(CH_3)_2 \quad (2)$$

In this ligand-exchange reaction, TMA accepts fluorine from the AlF_3 surface layer to form volatile $AlF(CH_3)_2$ species. $AlF(CH_3)_2$ is stable and has been shown to have a vapor pressure of 80 Torr at 100 °C.[53] Methyl groups from TMA are also transferred to the AlF_3 surface layer to form additional volatile $AlF(CH_3)_2$ reaction products. This ligand-exchange reaction removes Al−F species from the surface.

Negative absorbance features are also observed in Figure 8a at 1065 and 1220 cm^{-1} that are consistent with the loss of Si−O asymmetric stretching vibrations.[30] These absorbance losses are accompanied by absorbance gains at 845 and 1000 cm^{-1} that are attributed to the addition of Al−O and Al−O−Si stretching vibrations, respectively.[46−48,54,55] These absorbance changes are consistent with the reaction of TMA with SiO_2 to form Al_2O_3 and aluminosilicate surface species. The reaction of TMA with SiO_2 to form Al_2O_3 could occur according to

$$4Al(CH_3)_3 + 3SiO_2 \rightarrow 2Al_2O_3 + 3Si(CH_3)_4 \quad (3)$$

This reaction is predicted to be spontaneous with a Gibbs free energy change of $\Delta G = -235$ kcal/mol at 300 °C.[52] The reaction between TMA and SiO_2 has also been computed to be thermodynamically favorable using density functional theory methods.[56]

Infrared analysis, temperature-programmed desorption, and X-ray photoelectron spectroscopy have also been used to analyze the Si−methyl and Al−methyl surface species that result from the chemisorption of TMA on SiO_2. Above 175 °C, the aluminum alkyl surface complex has been shown to decompose, yielding more methyl groups bonded to silicon. At 325 °C, $Si-CH_3$ species were observed to react further to form volatile tetramethylsilane ($Si(CH_3)_4$) as suggested in eq 3.[41]

Previous studies have also investigated the reaction of Al with SiO_2.[57−59] Aluminum films deposited on thermally grown SiO_2 surfaces have been shown to reduce SiO_2 and yield Al_2O_3 and Si according to

$$4Al + 3SiO_2 \rightarrow 2Al_2O_3 + 3Si \quad (4)$$

This reaction is thermodynamically favorable with a Gibbs free energy value of $\Delta G = -68$ kcal/mol at 300 °C.[52] There are similarities between the reactions of TMA and Al with SiO_2. During thermal ALE, TMA may act like metallic aluminum to produce Al_2O_3 as expected for thermite reactions.[60]

Figure 8b shows the absorbance changes after a subsequent HF exposure. An absorbance gain at 675 cm^{-1} is accompanied by absorbance losses at 845 and 1000 cm^{-1}. These results are similar to those observed in Figure 7b and are consistent with HF exposures acting to fluorinate the Al_2O_3/aluminosilicate layer formed during TMA exposures. This fluorinated layer can then be removed during subsequent TMA exposures. TMA can also act to further displace silicon at the surface to form a new Al_2O_3/aluminosilicate layer that can then be etched during the subsequent ALE cycle.

5. FTIR Studies of Self-Limiting Behavior and Pressure Dependence. The self-limiting behavior of the TMA and HF reactions at a given reactant pressure was determined by monitoring the absorbance changes for the Si−O stretching vibrations between 1050 and 1225 cm^{-1} during TMA exposures and the Al−F stretching vibrations between 550 and 750 cm^{-1} during HF exposures. Figure 9 examines the self-limiting behavior of the SiO_2 ALE reactions with TMA and HF at 300 °C. Each data point was collected after a ~0.5 Torr static dose for 5 s.

Figure 9a displays the normalized integrated absorbance change for the Si−O stretching vibration between 1050 and 1225 cm^{-1} after TMA exposures. Self-limiting behavior is observed after a TMA exposure of 15 Torr s. The surface Al_2O_3/aluminosilicate layer acts as a diffusion barrier that limits Al diffusion through the layer to reach unreacted SiO_2. Figure 9b shows the normalized integrated absorbance change for the Al−F stretching vibrations between 550 and 750 cm^{-1} after HF exposures. Self-limiting behavior is observed after a HF exposure of 10 Torr s. The self-limiting behavior is consistent with the fluorination of the Al−O species that were added during previous TMA exposures. After all of the Al−O species are converted to Al−F species, no further reaction occurs.

DOI: 10.1021/acsami.7b01259
ACS Appl. Mater. Interfaces 2017, 9, 10296−10307

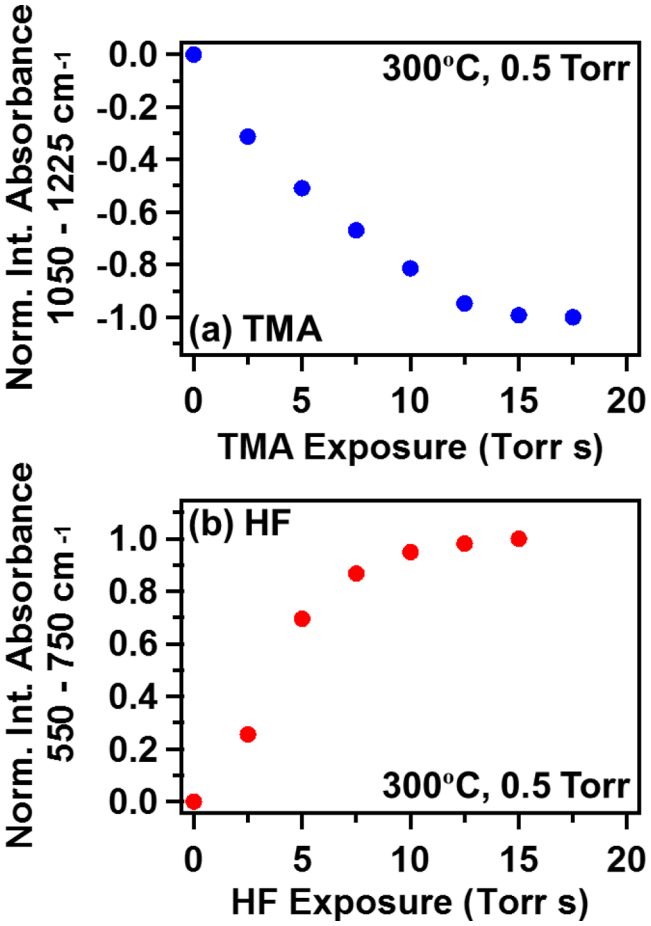

Figure 9. (a) Normalized integrated absorbance of the Si−O stretching vibration between 1050 and 1225 cm^{-1} during the TMA exposure. (b) Normalized integrated absorbance of the Al−F stretching vibration between 550 and 750 cm^{-1} during the HF exposure.

FTIR studies also observed the absorbance changes at different reactant pressures. Figure 10 displays the FTIR difference spectra between 450 and 1450 cm^{-1} for increasing TMA pressures at 300 °C. The difference spectra are referenced to the previous HF exposure. This previous exposure consisted of a ∼1 Torr static HF dose for 30 s. Figure 10a was obtained after a self-passivating reaction with a TMA static exposure of 0.5 Torr. The resulting vibrational features are similar to those presented in Figure 8. The TMA exposure of 0.5 Torr shows the loss of Al−F species at 675 cm^{-1} and Si−O−Si species at 1220 cm^{-1}. Absorbance gains are also observed at 845 and 1000 cm^{-1} that are consistent with the addition of Al−O and Si−O−Al species.

Figure 10b and Figure 10c show the resulting difference spectra when the TMA reactant pressure is increased to 1.0 and 4.0 Torr, respectively. These difference spectra were recorded after self-passivating reactions with TMA static exposures of 1.0 and 4.0 Torr, respectively. Little change is observed in the Al−F vibrational region. This behavior suggests that Al−F species are removed from the surface before Al reacts with the underlying SiO_2 layer. Further absorbance loss at 1220 cm^{-1} and absorbance gains at 845 and 1000 cm^{-1} are consistent with additional conversion of Si−O species to Al−O species at the higher TMA pressures.

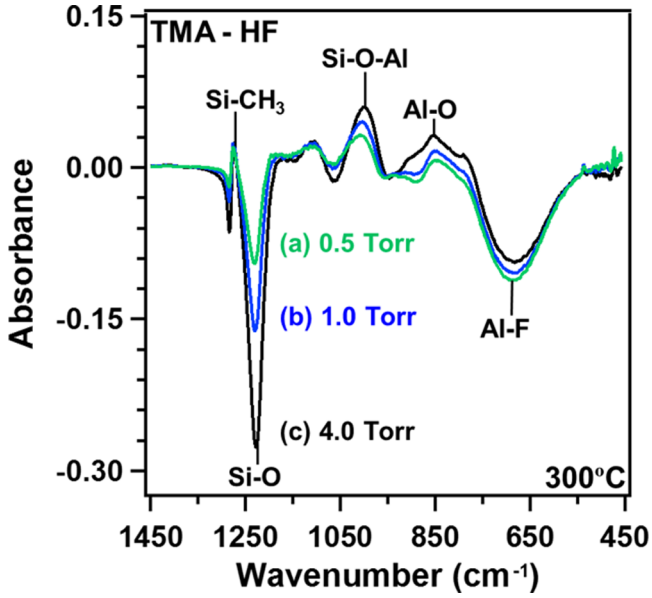

Figure 10. Difference infrared absorption spectra between 450 and 1450 cm^{-1} for increasing TMA pressures of (a) 0.5, (b) 1.0, and (c) 4.0 Torr at 300 °C. Difference spectra are referenced to the spectrum after the previous HF exposure at 1 Torr for 30 s.

Figure 11 shows the FTIR difference spectra between 450−1450 cm^{-1} for increasing HF pressures at 300 °C. The

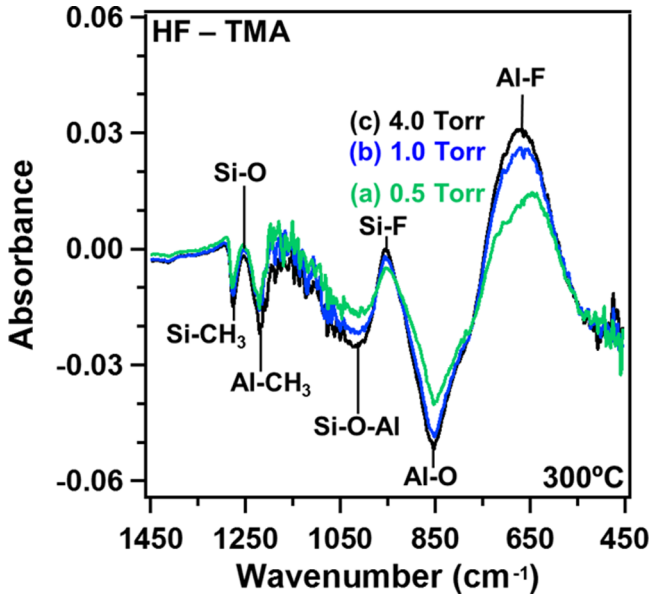

Figure 11. Difference infrared absorption spectra between 450 and 1450 cm^{-1} for increasing HF pressures of (a) 0.5. (b) 1.0. and (c) 4.0 Torr at 300 °C. Difference spectra are referenced to the spectrum after the previous TMA exposure at 1 Torr for 30 s.

difference spectra are referenced to the previous TMA exposure. This previous exposure consisted of a ∼1 Torr static TMA dose for 30 s. Figure 11a was obtained after a self-passivating reaction with a HF static exposure of 0.5 Torr. The HF exposure of 0.5 Torr causes absorbance losses at 845 and 1000 cm^{-1} and absorbance gains at 675 and 955 cm^{-1}. These absorbance changes are consistent with the conversion of Al−O and Si−O−Al species to Al−F and Si−F species, respectively.

DOI: 10.1021/acsami.7b01259
ACS Appl. Mater. Interfaces 2017, 9, 10296−10307

Figure 11b was collected after a self-passivating HF reaction when the HF pressure was increased to 1.0 Torr. Figure 11c was recorded after a self-passivating reaction when the HF pressure was increased further to 4.0 Torr. These spectra show additional Al−O and Si−O−Al to Al−F and Si−F conversion in each absorbance region at the higher HF pressures. The absorbance changes observed after the HF exposure at 4.0 Torr are much less than the absorbance changes observed after the HF exposures at 0.5 and 1.0 Torr. These results are consistent with a self-passivating fluorination reaction.

The self-passivating Al_2O_3/aluminosilicate and fluoride surface layers are similar to the self-passivating oxide layers that form on metal[61,62] or silicon[34,63,64] surfaces and protect the metal or silicon surfaces from further oxidation. These self-passivating reactions can be understood in terms of diffusion-limited growth. The surface layers act as diffusion barriers that limit the conversion and fluorination reactions. Diffusion-limited growth has been described earlier in the classic Deal−Grove treatment of silicon oxidation.[34]

In the Deal−Grove approach,[34] the flux of reactants, F, is dependent on the concentration gradient across the SiO_2 surface layer according to

$$F = D(C_0 - C_s)/x \quad (5)$$

where D is the diffusion coefficient, C_0 is the concentration of reactants on the SiO_2 surface, C_s is the concentration of reactants at the SiO_2/Si interface, and x is the thickness of the SiO_2 surface layer. Solution of the diffusion equations reveals that the thickness of the SiO_2 surface layer will increase parabolically versus time and display self-passivating behavior at longer times.[34]

The larger amounts of conversion and fluorination at higher pressures can also be understood in terms of diffusion-limited growth. The pressure dependence of the thickness is determined by C_0, the concentration of reactants on the surface. C_0 is defined by the reactant pressure, P, and the Henry's law constant, H, according to $C_0 = HP$. Higher pressures lead to higher surface reactant concentrations. These higher concentrations produce larger concentration gradients across the surface layer and thicker surface layers.

6. XPS Studies of Silicon Oxidation State after TMA and HF Reactions with SiO_2. The reaction of TMA with SiO_2 given by eq 3 reduces silicon because CH_3 is much less electronegative than oxygen. The CH_3 group has an electronegativity of $\chi = 2.525$.[65] In contrast, oxygen has an electronegativity of $\chi = 3.5$. The reaction of TMA with SiO_2 will lead to more electron density on silicon in the $SiO_{4-y}(CH_3)_y$ suboxide products.

The reduction of SiO_2 and formation of Al_2O_3/aluminosilicates after TMA exposure were observed by ex situ XPS analysis. Figure 12 displays the Si 2p XPS spectra of (a) bare SiO_2, (b) SiO_2 after an 8 Torr TMA exposure for 5 min at 300 °C, and (c) SiO_2 after an 8 Torr TMA exposure for 5 min followed by a 4 Torr HF exposure for 10 min at 300 °C. The higher reactant pressures and exposure times were chosen to ensure that changes in the surface species were detectable by XPS analysis.

The Si 2p peaks in Figure 12 were deconvoluted into silicon oxidation states of 4+, 3+, 2+, 1+, and 0. The fits were constrained by the fwhm and binding energies of the individual Si oxidation states as described in section II.1. The binding energies of the silicon oxidation states of 4+, 3+, 2+, 1+, and 0 are shown by the dashed lines in Figure 12.[25−27] Figure 12a depicts the SiO_2 control sample with a broad peak at 104.3 eV. This peak position is consistent with literature values for SiO_2 and silicon atoms in the Si^{4+} oxidation state.[66]

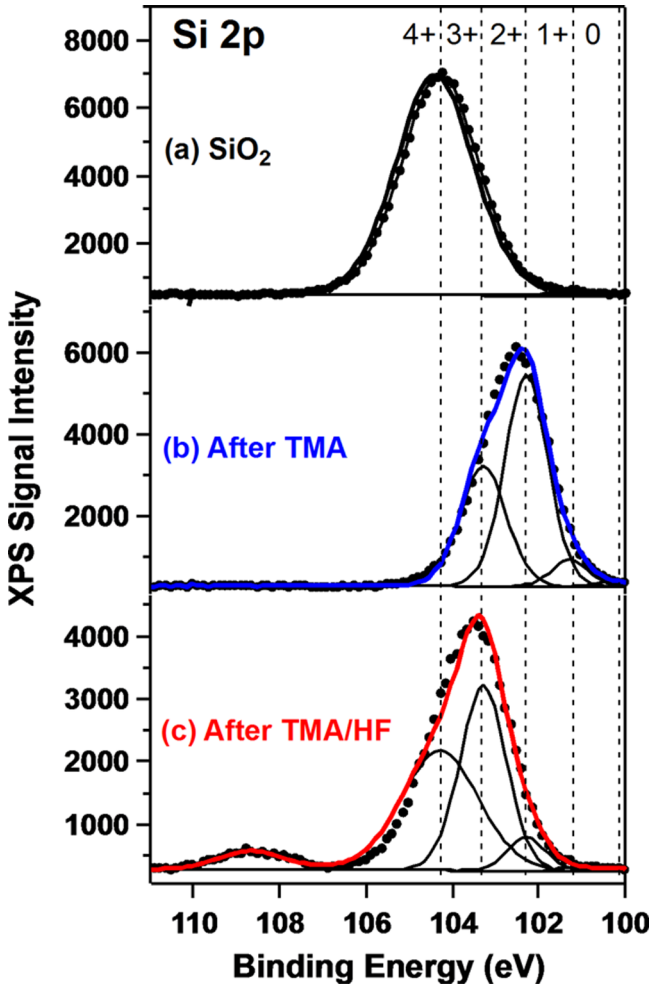

Figure 12. XPS results for the Si 2p peak from (a) initial SiO_2 film, (b) SiO_2 film after TMA exposure, and (c) SiO_2 film after TMA and HF exposures. The dashed lines correspond to the 4+, 3+, 2+, 1+, and 0 oxidation states for the Si 2p peak.

Figure 12b shows the results after the TMA exposure. The Si 2p peak shifts to lower binding energies centered around 102.5 eV that is composed of 3+, 2+, and 1+ oxidation states. The disappearance of the 4+ oxidation state indicates the TMA exposure reduces the Si^{4+} in SiO_2 into Si suboxides. As suggested by the reaction in eq 3, these silicon suboxides may be $SiO_3(CH_3)$, $SiO_2(CH_3)_2$, and $SiO(CH_3)_3$ surface species.

Figure 12c displays the XPS results for the Si 2p peak after sequential TMA and HF exposures. The HF exposure shifts the Si 2p peak back to higher energies and can be deconvoluted into silicon oxidation states of 4+, 3+, and 2+. These higher silicon oxidation states are consistent with HF reacting with $SiCH_3$ surface species according to $SiCH_3 + HF \rightarrow SiF + CH_4$. This reaction could form $SiFO_3$, $SiFO_2(CH_3)$, and $SiFO(CH_3)_2$ surface species with silicon oxidation states of 4+, 3+, and 2+, respectively. These higher oxidation states are expected because fluorine has a high electronegativity of $\chi = 4.0$. In addition, Figure 12c also displays a higher energy peak at 108.8 eV. This higher energy peak can be attributed to a shake-up satellite peak.[67] Shake-up satellite peaks can occur when the emitted photoelectron excites an ion. These shake-up peaks from Si 2p

DOI: 10.1021/acsami.7b01259
ACS Appl. Mater. Interfaces 2017, 9, 10296−10307

can be observed when Si is present in a siloxane polymer structure.[67]

The reduction of SiO_2 and formation of Al_2O_3/aluminosilicates after TMA exposure were also monitored by XPS analysis of the Si 2p XPS spectra after a 4 Torr TMA exposure on SiO_2 for 20 s at 300 °C. The Si 2p XPS spectra displayed a shift from the 4+ oxidation state for SiO_2 to a distribution of 4+, 3+, 2+, and 1+ oxidation states after the TMA exposure. The peak of the spectrum occurred at the 3+ oxidation state compared with a peak at the 2+ oxidation state for the TMA exposure at 8 Torr shown in Figure 12b. The Si 2p XPS spectrum after a 4 Torr TMA exposure on SiO_2 for 20 s followed by a 4 Torr HF exposure for 20 s at 300 °C displayed a shift back to higher oxidation states similar to the results shown in Figure 12c.

The Al 2p XPS peak was also consistent with the formation of Al_2O_3 at the surface after TMA exposure. Figure 13a and

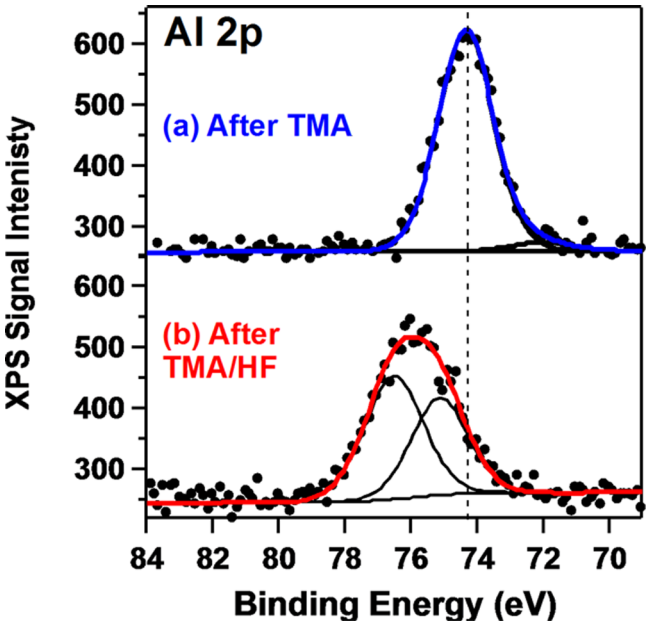

Figure 13. XPS results for the Al 2p peak from (a) SiO_2 film after TMA exposure and (b) SiO_2 film after TMA and HF exposures. These XPS spectra were obtained from the same samples as shown in Figure 12. The dashed line corresponds to the binding energy for Al in Al_2O_3.

Figure 13b show the Al 2p XPS spectra after the TMA exposure and after sequential TMA and HF exposures, respectively. These XPS spectra were obtained from the same samples as shown in Figure 12. Figure 13a displays a peak at 74.3 eV after the TMA exposure that corresponds to the formation of Al_2O_3 or aluminosilicates.[66,68] There is also a smaller shoulder on this peak at ~72 eV that corresponds to more metallic Al. This peak may result from some TMA decomposition.[69]

Figure 13b shows that the Al 2p XPS peak shifts to higher binding energies after sequential TMA and HF exposures. The broader peak at ~76 eV is consistent with the fluorination of Al_2O_3.[68] This peak may be composed of AlF_3 at 77 eV and oxyaluminum fluoride species at lower energies.[66,68] Oxygen is less electronegative and will not shift the Al 2p binding energy as much as fluorine.

7. Mechanism for SiO_2 ALE and Future Possibilities. A simplified schematic for the proposed SiO_2 ALE chemistry during the sequential TMA and HF exposures on SiO_2 is shown in Figure 14. After the first TMA and HF exposures, subsequent TMA exposures react with the AlF_3 species on the

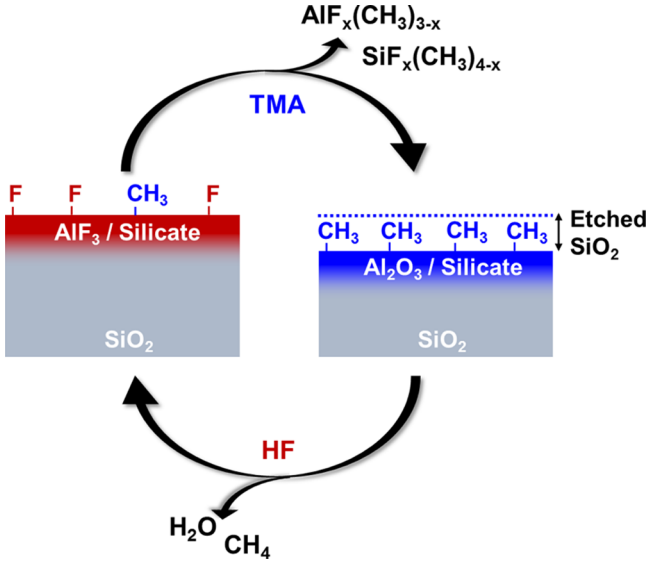

Figure 14. Schematic of the proposed reaction mechanism for SiO_2 ALE showing the sequential TMA and HF reactions.

SiO_2 substrate to form volatile $AlF(CH_3)_2$ etch products. After removal of the AlF_3 species, TMA reacts with the underlying SiO_2 to form Al_2O_3 and aluminosilicates with the possible release of $Si(CH_3)_4$ or $Si(CH_3)_xF_{4-x}$, as volatile reaction products. Mass spectrometry studies are required to confirm the volatile reaction products. In addition, suboxides such as $AlO_{3-x}(CH_3)_x$ where $x = 1$ or 2 and $SiO_{4-y}(CH_3)_y$ where $y = 1$, 2, or 3 may be present in the surface layer.

The subsequent HF exposures converts the Al_2O_3 and aluminosilicates to AlF_3 and releases H_2O as a volatile reaction product. The $AlO_{3-x}(CH_3)_x$ and $SiO_{4-y}(CH_3)_y$ suboxides may also lead to the formation of CH_4 during the HF exposure. Moreover, silicon species such as $SiFO_3$, $SiFO_2(CH_3)$, and $SiFO(CH_3)_2$ may be produced in the near surface layer. The shake-up satellite XPS peak from Si 2p also suggests that the Si may be in polymer structures similar to siloxane.

The basics of this mechanism are similar to the recently observed "conversion-etch" mechanism for ZnO ALE.[23] For ZnO ALE, TMA exposures converted ZnO to Al_2O_3. HF exposures then fluorinated the Al_2O_3 to AlF_3. Subsequent TMA exposures removed the AlF_3 and converted more ZnO to Al_2O_3.[23] ZnO ALE by the "conversion-etch" mechanism occurred at lower reactant pressures of 60−80 mTorr. In contrast to the results for SiO_2 ALE, higher reactant pressures of >0.1 Torr were not required for ZnO ALE.

The lower pressures for ZnO ALE suggest that "conversion-etch" may be more favorable for ZnO ALE than SiO_2 ALE. However, thermochemical calculations do not support this viewpoint. The free energy change for the reaction $3ZnO + 2Al(CH_3)_3 \rightarrow Al_2O_3 + 3Zn(CH_3)_2$ is $\Delta G = -168$ kcal at 300 °C.[52] In comparison, the free energy change for the reaction $1.5SiO_2 + 2Al(CH_3)_3 \rightarrow Al_2O_3 + 1.5Si(CH_3)_4$ is $\Delta G = -197$ kcal at 300 °C.[52] There must be other kinetic factors that favor ZnO ALE by the "conversion-etch" mechanism.

The "conversion-etch" mechanism may be general and may be realized when the metal oxide formed by the conversion reaction is more stable than the initial metal oxide. Guidelines

DOI: 10.1021/acsami.7b01259
ACS Appl. Mater. Interfaces 2017, 9, 10296−10307

for determining the relative stability of metal oxides can be obtained from thermochemical calculations or Ellingham diagrams.[70] Some materials may not have viable pathways for thermal ALE because the ligand-exchange reactions may not produce stable and volatile reaction products.[20] By converting the initial material to a different material, the "conversion-etch" mechanism may enlarge the number of materials that can be etched using thermal ALE. For example, TMA is anticipated to convert other metal oxides, such as SnO_2 and In_2O_3, to Al_2O_3.[23] Thermal Al_2O_3 ALE has been demonstrated using HF and either $Sn(acac)_2$ or TMA as the reactants.[17−19] Likewise, TMA is expected to convert various nitrides, such as Si_3N_4, to AlN.[23] Thermal AlN ALE has been demonstrated using HF and $Sn(acac)_2$ as the reactants.[21]

Thermal SiO_2 ALE also suggests a possible procedure for thermal Si ALE. The silicon surface can first be oxidized to form a self-passivating oxide layer on the silicon surface.[63,64] The resulting SiO_2 layer can then be etched by the "conversion-etch" mechanism using sequential TMA and HF exposures. By repetition of the silicon oxidation and sequential TMA and HF exposures, silicon should be etched with atomic layer precision. Similar procedures may also be defined for the thermal ALE of metals using sequential oxidation, fluorination, and ligand-exchange reactions.

IV. CONCLUSIONS

Sequential reactions of trimethylaluminum (TMA) and hydrogen fluoride (HF) were employed for the thermal atomic layer etching (ALE) of SiO_2 at 300 °C. The etch rates during SiO_2 ALE were dependent on reactant pressures. SiO_2 etch rates of 0.027, 0.15, 0.20, and 0.31 Å/cycle were observed at static reactant pressures of 0.1, 0.5, 1.0, and 4.0 Torr, respectively, by ex situ X-ray reflectivity measurements. A similar increase in SiO_2 etch rate with reactant pressure was confirmed by ex situ spectroscopic ellipsometry measurements. The pressure dependence of the etch rate for SiO_2 ALE was also observed by in situ FTIR studies. In addition, the FTIR measurements monitored the pressure-dependent conversion of the SiO_2 surface to an Al_2O_3/aluminosilicate layer. Ex situ XPS measurements also monitored the reduction of the silicon oxidation state after the TMA reaction.

The Al_2O_3/aluminosilicate intermediate is attributed to the conversion of SiO_2 to Al_2O_3 and reduced silicon species by the TMA exposure according to reactions like $3SiO_2 + 4Al(CH_3)_3 \rightarrow 2Al_2O_3 + 3Si(CH_3)_4$. The HF exposure can then fluorinate Al_2O_3 to AlF_3 and form silicon fluoride species after this conversion reaction. Subsequently, the next TMA exposure can remove AlF_3 by a ligand-exchange transmetalation reaction and then convert additional SiO_2 to Al_2O_3 and reduced silicon species. The sequential TMA and HF reactions lead to SiO_2 ALE because the individual TMA and HF reactions display self-limiting behavior at the various reactant pressures.

The pressure-dependent conversion reaction of the SiO_2 surface to an Al_2O_3/aluminosilicate layer by TMA is critical for thermal SiO_2 ALE. The "conversion-etch" mechanism for SiO_2 ALE is observed at reactant pressures of >0.1 Torr. Other conversion reactions will be able to transform initial materials that cannot be etched to different materials that may have possible etching pathways. The "conversion-etch" mechanism will increase the number of materials that can be etched by thermal ALE methods. Oxidation and conversion reactions may also lead to procedures for thermal Si ALE.

AUTHOR INFORMATION

Corresponding Author

*E-mail: steven.george@colorado.edu. Phone: 303-492-3398. Fax: 303-492-5894.

ORCID

Steven M. George: 0000-0003-0253-9184

Notes

The authors declare no competing financial interest.

ACKNOWLEDGMENTS

This research was funded by the National Science Foundation by Grants CHE-1306131 and CHE-1609554 and the Defense Advanced Projects Agency (DARPA) by Grant W911NF-13-1-0041. The authors thank Huaxing Sun for the XPS measurements. The authors also thank Joel Clancey for assistance with the TEM analysis of the silicon nanoparticles.

REFERENCES

(1) Nojiri, K. *Dry Etching Technology for Semiconductors*; Springer: Heidelberg, Germany, 2012.

(2) Carver, C. T.; Plombon, J. J.; Romero, P. E.; Suri, S.; Tronic, T. A.; Turkot, R. B. Atomic Layer Etching: An Industry Perspective. *ECS J. Solid State Sci. Technol.* **2015**, *4*, N5005−N5009.

(3) Blumberg, A. A.; Stavrinou, S. C. Tabulated Functions for Heterogeneous Reaction Rates - The Attack of Vitreous Silica by Hydrofluoric Acid. *J. Phys. Chem.* **1960**, *64*, 1438−1442.

(4) Monk, D. J.; Soane, D. S.; Howe, R. T. A Review of the Chemical Reaction Mechanisma and Kinetics for Hydrofluoric Acid Etching of Silicon Dioxide for Surface Micromachining Applications. *Thin Solid Films* **1993**, *232*, 1−12.

(5) Spierings, G. A. C. M. Wet Chemical Etching of SIlicate-Glasses in Hydrofluoric Acid Based Solutions. *J. Mater. Sci.* **1993**, *28*, 6261−6273.

(6) Knotter, D. M. Etching Mechanism of Vitreous Silicon Dioxide in HF-Based Solutions. *J. Am. Chem. Soc.* **2000**, *122*, 4345−4351.

(7) Helms, C. R.; Deal, B. E. Mechanisms of the HF/H_2O Vapor Phase Etching of SiO_2. *J. Vac. Sci. Technol., A* **1992**, *10*, 806−811.

(8) Vanderheide, P. A. M.; Baan Hofman, M. J.; Ronde, H. J. Etching of Thin SiO_2 Layers Using Wet HF Gas. *J. Vac. Sci. Technol., A* **1989**, *7*, 1719−1723.

(9) Kang, J. K.; Musgrave, C. B. The Mechanism of HF/H_2O Chemical Etching of SiO_2. *J. Chem. Phys.* **2002**, *116*, 275−280.

(10) Mogab, C. J.; Adams, A. C.; Flamm, D. L. Plasma Etching of Si and SiO_2 - Effect of Oxygen Additions to CF_4 Plasmas. *J. Appl. Phys.* **1978**, *49*, 3796−3803.

(11) Rueger, N. R.; Beulens, J. J.; Schaepkens, M.; Doemling, M. F.; Mirza, J. M.; Standaert, T.; Oehrlein, G. S. Role of Steady State Fluorocarbon Films in the Etching of Silicon Dioxide using CHF_3 in an Inductively Coupled Plasma Reactor. *J. Vac. Sci. Technol., A* **1997**, *15*, 1881−1889.

(12) Zhang, D.; Kushner, M. J. Investigations of Surface Reactions during C_2F_6 Plasma Etching of SiO_2 with Equipment and Feature Scale Models. *J. Vac. Sci. Technol., A* **2001**, *19*, 524−538.

(13) Metzler, D.; Bruce, R. L.; Engelmann, S.; Joseph, E. A.; Oehrlein, G. S. Fluorocarbon Assisted Atomic Layer Etching of SiO_2 using Cyclic Ar/C_4F_8 Plasma. *J. Vac. Sci. Technol., A* **2014**, *32*, 020603.

(14) Oehrlein, G. S.; Metzler, D.; Li, C. Atomic Layer Etching at the Tipping Point: An Overview. *ECS J. Solid State Sci. Technol.* **2015**, *4*, N5041−N5053.

(15) Lee, Y.; DuMont, J. W.; George, S. M. Atomic Layer Etching of HfO_2 Using Sequential, Self-Limiting Thermal Reactions with $Sn(acac)_2$ and HF. *ECS J. Solid State Sci. Technol.* **2015**, *4*, N5013−N5022.

(16) Lee, Y.; DuMont, J. W.; George, S. M. Atomic Layer Etching of AlF_3 Using Sequential, Self-Limiting Thermal Reactions with Sn-

DOI: 10.1021/acsami.7b01259
ACS Appl. Mater. Interfaces 2017, 9, 10296−10307

(acac)$_2$ and Hydrogen Fluoride. *J. Phys. Chem. C* **2015**, *119*, 25385−25393.
(17) Lee, Y.; DuMont, J. W.; George, S. M. Mechanism of Thermal Al_2O_3 Atomic Layer Etching Using Sequential Reactions with Sn(acac)$_2$ and HF. *Chem. Mater.* **2015**, *27*, 3648−3657.
(18) Lee, Y.; DuMont, J. W.; George, S. M. Trimethylaluminum as the Metal Precursor for the Atomic Layer Etching of Al_2O_3 Using Sequential, Self-Limiting Thermal Reactions. *Chem. Mater.* **2016**, *28*, 2994−3003.
(19) Lee, Y.; George, S. M. Atomic Layer Etching of Al_2O_3 Using Sequential, Self-Limiting Thermal Reactions with Sn(acac)$_2$ and HF. *ACS Nano* **2015**, *9*, 2061−2070.
(20) Lee, Y.; Huffman, C.; George, S. M. Selectivity in Thermal Atomic Layer Etching Using Sequential, Self-Limiting Fluorination and Ligand-Exchange Reactions. *Chem. Mater.* **2016**, *28*, 7657−7665.
(21) Johnson, N. R.; Sun, H.; Sharma, K.; George, S. M. Thermal Atomic Layer Etching of Crystalline Aluminum Nitride Using Sequential, Self-Limiting Hydrogen Fluoride and Sn(acac)$_2$ Reactions and Enhancement by H_2 and Ar Plasmas. *J. Vac. Sci. Technol., A* **2016**, *34*, 050603.
(22) George, S. M.; Lee, Y. Prospects for Thermal Atomic Layer Etching Using Sequential, Self-Limiting Fluorination and Ligand-Exchange Reactions. *ACS Nano* **2016**, *10*, 4889−4894.
(23) Zywotko, D. R.; George, S. M. Thermal Atomic Layer Etching of ZnO by a "Conversion-Etch" Mechanism Using Sequential Exposures of Hydrogen Fluoride and Trimethylaluminum. *Chem. Mater.* **2017**, *29*, 1183−1191.
(24) Elam, J. W.; Groner, M. D.; George, S. M. Viscous Flow Reactor with Quartz Crystal Microbalance for Thin Film Growth by Atomic Layer Deposition. *Rev. Sci. Instrum.* **2002**, *73*, 2981−2987.
(25) Bell, F. G.; Ley, L. Photoemission Study of SiO_x (0< x <2) Alloys. *Phys. Rev. B: Condens. Matter Mater. Phys.* **1988**, *37*, 8383−8393.
(26) Saito, Y. Adsorption of Anhydrous Hydrogen Fluoride onto Silicon and Native Oxide by XPS. *Surf. Sci. Spectra* **1999**, *6*, 228−236.
(27) Kim, S.; Kim, M. C.; Choi, S. H.; Kim, K. J.; Hwang, H. N.; Hwang, C. C. Size Dependence of Si 2p Core-level Shift at Si Nanocrystal/SiO_2 Interfaces. *Appl. Phys. Lett.* **2007**, *91*, 103113.
(28) DuMont, J. W.; George, S. M. Pyrolysis of Alucone Molecular Layer Deposition Films Studied Using In Situ Transmission Fourier Transform Infrared Spectroscopy. *J. Phys. Chem. C* **2015**, *119*, 14603−14612.
(29) Ferguson, J. D.; Weimer, A. W.; George, S. M. Atomic Layer Deposition of Ultrathin and Conformal Al_2O_3 films on BN Particles. *Thin Solid Films* **2000**, *371*, 95−104.
(30) Queeney, K. T.; Weldon, M. K.; Chang, J. P.; Chabal, Y. J.; Gurevich, A. B.; Sapjeta, J.; Opila, R. L. Infrared Spectroscopic Analysis of the Si/SiO_2 Interface Structure of Thermally Oxidized Silicon. *J. Appl. Phys.* **2000**, *87*, 1322−1330.
(31) Devine, R. A. B. Structural Nature of the Si/SiO_2 Interface Through Infrared Spectroscopy. *Appl. Phys. Lett.* **1996**, *68*, 3108−3110.
(32) Mawhinney, D. B.; Glass, J. A.; Yates, J. T. FTIR Study of the Oxidation of Porous Silicon. *J. Phys. Chem. B* **1997**, *101*, 1202−1206.
(33) Ogata, Y.; Niki, H.; Sakka, T.; Iwasaki, M. Oxidation of Porous Silicon Unver Water Vapor Environment. *J. Electrochem. Soc.* **1995**, *142*, 1595−1601.
(34) Deal, B. E.; Grove, A. S. General Relationship for Thermal Oxidation of Silicon. *J. Appl. Phys.* **1965**, *36*, 3770−3778.
(35) Bhat, V. K.; Pattabiraman, M.; Bhat, K. N.; Subrahmanyam, A. The Growth of Ultrathin Oxides of Silicon by Low Temperature Wet Oxidation Technique. *Mater. Res. Bull.* **1999**, *34*, 1797−1803.
(36) Gupta, P.; Colvin, V. L.; George, S. M. Hydrogen Desorption Kinetics from Monohydride and Dihydride Species on Silicon Surfaces. *Phys. Rev. B: Condens. Matter Mater. Phys.* **1988**, *37*, 8234−8243.
(37) Koehler, B. G.; Mak, C. H.; Arthur, D. A.; Coon, P. A.; George, S. M. Desorption Kinetics of Hydrogen and Deuterium from Si(111)7x7 Studied Using Laser Induced Thermal Desorption. *J. Chem. Phys.* **1988**, *89*, 1709−1718.
(38) Gupta, P.; Mak, C. H.; Coon, P. A.; George, S. M. Oxidation Kinetics of Si(111)7x7 in the Submonolayer Regime. *Phys. Rev. B: Condens. Matter Mater. Phys.* **1989**, *40*, 7739−7749.
(39) Koehler, B. G.; Mak, C. H.; George, S. M. Decomposition of H_2O on Si(111)7x7 Studied Using Laser Induced Thermal Desorption. *Surf. Sci.* **1989**, *221*, 565−589.
(40) Bellamy, L. J. *The Infra-Red Spectra of Complex Molecules*; Chapman and Hall: London, 1975.
(41) Bartram, M. E.; Michalske, T. A.; Rogers, J. W. A Reexamination of the Chemisorption of Trimethylaluminum on Silica. *J. Phys. Chem.* **1991**, *95*, 4453−4463.
(42) Puurunen, R. L.; Root, A.; Haukka, S.; Iiskola, E. I.; Lindblad, M.; Krause, A. O. I. IR and NMR Study of the Chemisorption of Ammonia on Trimethylaluminum-Modified Silica. *J. Phys. Chem. B* **2000**, *104*, 6599−6609.
(43) Yates, D. J. C.; Dembinski, G. W.; Kroll, W. R.; Elliott, J. J. Infrared Studies of Reactions between Silica and Trimethylaluminum. *J. Phys. Chem.* **1969**, *73*, 911−921.
(44) Morrow, B. A.; McFarlan, A. J. Surface Vibrational Modes of Silanol Groups on Silica. *J. Phys. Chem.* **1992**, *96*, 1395−1400.
(45) Grill, A.; Neumayer, D. A. Structure of Low Dielectric Constant to Extreme Low Dielectric Constant SiCOH Films: Fourier Transform Infrared Spectroscopy Characterization. *J. Appl. Phys.* **2003**, *94*, 6697−6707.
(46) Frank, M. M.; Chabal, Y. J.; Green, M. L.; Delabie, A.; Brijs, B.; Wilk, G. D.; Ho, M. Y.; da Rosa, E. B. O.; Baumvol, I. J. R.; Stedile, F. C. Enhanced Initial Growth of Atomic Layer Deposited Metal Oxides on Hydrogen-Terminated Silicon. *Appl. Phys. Lett.* **2003**, *83*, 740−742.
(47) Frank, M. M.; Chabal, Y. J.; Wilk, G. D. Nucleation and Interface Formation Mechanisms in Atomic Layer Deposition of Gate Oxides. *Appl. Phys. Lett.* **2003**, *82*, 4758−4760.
(48) Mackenzie, K. J. Infrared Frequency Calculations for Ideal Mullite ($3Al_2O_3.2SiO_2$). *J. Am. Ceram. Soc.* **1972**, *55*, 68−71.
(49) Kinney, J. B.; Staley, R. H. Reactions of Titanium Tetrachloride and Trimethylaluminum at Silica Surfaces Studies by Using Infrared Photo-acoustic Spectroscopy. *J. Phys. Chem.* **1983**, *87*, 3735−3740.
(50) Barabash, R. M.; Zaitsev, V. N.; Kovalchuk, T. V.; Sfihi, H.; Fraissard, J. Low-Temperature Fluorination of Silica by a Nonaqueous Solution of NH_4F. *J. Phys. Chem. A* **2003**, *107*, 4497−4505.
(51) Gross, U.; Ruediger, S.; Kemnitz, E.; Brzezinka, K.-W.; Mukhopadhyay, S.; Bailey, C.; Wander, A.; Harrison, N. Vibrational Analysis Study of Aluminum Trifluoride Phases. *J. Phys. Chem. A* **2007**, *111*, 5813−5819.
(52) *HSC Chemistry. HSC Chemistry 5.1*; Outokumpu Research Oy: Pori, Finland.
(53) Weidlein, J.; Krieg, V. Vibrational Spectra of Dimethyl and Diethyl Aluminum Fluoride. *J. Organomet. Chem.* **1968**, *11*, 9−16.
(54) Morozova, N. B.; Zherikova, K. V.; Baidina, I. A.; Sysoev, S. V.; Semyannikov, P. P.; Yakovkina, L. V.; Smirnova, T. P.; Gelfond, N. V.; Igumenov, I. K.; Carta, G.; Rossetto, G. Volatile Hafnium(IV) Compounds with Beta-Diketonate and Cyclopentadienyl Derivatives. *J. Phys. Chem. Solids* **2008**, *69*, 673−679.
(55) Mozgawa, W.; Sitarz, M.; Rokita, M. Spectroscopic Studies of Different Aluminosilicate Structures. *J. Mol. Struct.* **1999**, *511*, 251−257.
(56) Lamagna, L.; Wiemer, C.; Perego, M.; Spiga, S.; Rodriguez, J.; Coll, D. S.; Grillo, M. E.; Klejna, S.; Elliott, S. D. Mechanisms for Substrate-Enhanced Growth during the Early Stages of Atomic Layer Deposition of Alumina onto Silicon Nitride Surfaces. *Chem. Mater.* **2012**, *24*, 1080−1090.
(57) Bauer, R. S.; Bachrach, R. Z.; Brillson, L. J. Au and Al Interface Reactions with SiO_2. *Appl. Phys. Lett.* **1980**, *37*, 1006−1008.
(58) Hecht, M. H.; Vasquez, R. P.; Grunthaner, F. J.; Zamani, N.; Maserjian, J. A Novel X-ray Photoelectron Spectroscopy Study of the Al/SiO_2 Interface. *J. Appl. Phys.* **1985**, *57*, 5256−5262.

DOI: 10.1021/acsami.7b01259
ACS Appl. Mater. Interfaces 2017, 9, 10296−10307

(59) Tsukada, M.; Ohfuji, S. I. In Situ X-Ray Photoemission Spectroscopic Studies of Al/SiO_2 Interface Formation. *J. Vac. Sci. Technol., A* **1994**, *12*, 1−6.
(60) Wang, L. L.; Munir, Z. A.; Maximov, Y. M. Thermite Reactions - Their Utilization in the Synthesis and Processing of Materials. *J. Mater. Sci.* **1993**, *28*, 3693−3708.
(61) Graham, M. J.; Cohen, M. On the Mechanism of Low Temperature Oxidation (23-450 C) of Polycrystalline Nickel. *J. Electrochem. Soc.* **1972**, *119*, 879−882.
(62) Song, S.; Placido, F. Investigation on Initial Oxidation Kinetics of Al, Ni, and Hf Metal Film Surfaces. *Chin. Opt. Lett.* **2010**, *8* (Suppl.), 87−90.
(63) Derrie, J.; Commandre, M. SiO_2 Ultra Thin Film Growth Kinetics as Investigated by Surface Techniques. *Surf. Sci.* **1982**, *118*, 32−46.
(64) Fehlner, F. P. Formation of Ultrathin Oxide Films on Silicon. *J. Electrochem. Soc.* **1972**, *119*, 1723−1727.
(65) Matsunaga, N.; Rogers, D. W.; Zavitsas, A. A. Pauling's Electronegativity Equation and a New Corollary Accurately Predict Bond Dissociation Enthalpies and Enhance Current Understanding of the Nature of the Chemical Bond. *J. Org. Chem.* **2003**, *68*, 3158−3172.
(66) *NIST X-ray Photoelectron Spectroscopy Database*, version 4.1; National Institute of Standards and Technology: Gaithersburg, MD, 2012; http://srdata.nist.gov/xps/.
(67) Gardella, J. A.; Ferguson, S. A.; Chin, R. L. $\pi^* \leftarrow \pi$ Shakeup Satellites for the Analysis of Structure and Bonding in Aromatic Polymers by X-ray Photoelectron Spectroscopy. *Appl. Spectrosc.* **1986**, *40*, 224−232.
(68) Bose, O.; Kemnitz, E.; Lippitz, A.; Unger, W. E. S. C 1s and Au $4f_{7/2}$ Referenced XPS Binding Energy Data Obtained with Different Aluminium Oxides, -Hydroxides and -Fluorides. *Fresenius' J. Anal. Chem.* **1997**, *358*, 175−179.
(69) Mayer, T. M.; Rogers, J. W.; Michalske, T. A. Mechanism of Nucleation and Atomic Layer Growth of AlN on Si. *Chem. Mater.* **1991**, *3*, 641−646.
(70) Ellingham, H. J. T. Reducibility of Oxides and Sulphides in Metallurgical Processes. *J. Soc. Chem. Ind. London* **1944**, *63*, 125−133.

DOI: 10.1021/acsami.7b01259
ACS Appl. Mater. Interfaces 2017, 9, 10296−10307